Available online at www.sciencedirect.com
SCIENCE DIRECT®
International Journal of Rock Mechanics & Mining Sciences 42 (2005) 667–679
International Journal of Rock Mechanics and Mining Sciences
www.elsevier.com/locate/ijrmms

Double structure THM analyses of a heating test in a fractured tuff incorporating intrinsic permeability variations

S. Olivella*, A. Gens

Department of Geotechnical Engineering and Geosciences, Escola Tècnica Superior d'Enginyers de Camins, Canals i Ports, Universitat Politècnica de Catalunya (UPC), c/Jordi Girona 1-3, Edificio D-2, 08034 Barcelona, Spain

Accepted 2 March 2005
Available online 4 May 2005

Abstract

This paper presents thermo-hydro-mechanical (THM) analyses simulating the Drift Scale Test (DST) performed at Yucca Mountain. A double structure approach based on two superimposed domains is adopted. Intrinsic permeability changes with deformations imply full THM coupling. Temperatures and gas permeabilities were measured during 4 years and are used to validate the model. Measured gas permeability variations show patterns that are successfully explained by the model calculations. These gas permeability variations may be attributed to thermo-hydraulic effects, and also to mechanical effects. Different cases of intrinsic permeability variations have been considered in the model and their influence on the calculated temperatures, degree of saturations and gas permeabilities are presented. Volumetric deformation, in contraction or dilatancy, implies changes in the aperture of rock fractures that in turn lead to changes in intrinsic permeability. Dilatancy, caused by shear stresses, increases intrinsic permeability. Consideration of this factor contributes significantly to improve the agreement of calculated gas permeability with the measured values obtained during the DST experiment.

Keywords: THM analysis; Fractured rock; Double structure; Permeability; Gas flow

1. Introduction

The in situ heating test Drift Scale Test (DST) performed at Yucca Mountain is a challenging modelling problem because it involves several coupled phenomena, concerning multiphase fluid flow in a deformable rock. The in situ DST consists of a 47.5 m long, 5 m diameter drift heated by nine heaters simulating waste canisters placed on the floor. Additional heat is supplied by 50 wing heaters inserted into horizontal boreholes drilled into each side wall [1,2]. Temperatures above 200 °C are achieved at some points.

Thermal–hydrological simulations have been performed by Birkholzer and Tsang [3] using the finite volume simulator TOUGH2 [4,5]. These involve three-dimensional (3D) analyses and the simulation covers 400 days which is the time for which measurements were available at the moment the model was developed. The thermo-hydrological model presented by these authors has served as a relevant reference for the work presented here. Most for thermo-hydrological parameters have been taken from these authors [3].

In other reports containing modelling contributions of the DST test, thermo-mechanical calculations were performed in two dimensions using the calculated temperatures from the 3D thermo-hydrological models as input data for the mechanical calculations [2]. The coupling considered in those calculations was only in one direction, although temperatures were influenced by the hydrological processes and vice versa; the thermo-hydrological problem was not influenced by deformations, but deformations were influenced by the thermal

*Corresponding author. Tel.: +34 934017253; fax: +34 934017251.
E-mail addresses: Sebastia.olivella@upc.es (S. Olivella), Antonio.Gens@upc.edu (A. Gens).

1365-1609/$ - see front matter © 2005 Elsevier Ltd. All rights reserved.
doi:10.1016/j.ijrmms.2005.03.007

field. However, one can expect that water and air flow, which are controlled by intrinsic permeability, will be influenced by deformations. Consequently, the temperature field may be modified because thermal conductivity is a function of water content and because heat is transported by advection due to fluid flows.

Thermo-hydro-mechanical (THM) investigations and modelling are a subject of increasing interest, especially in problems related to waste disposal. For instance, Rutqvist et al. [6] present a comparison of programs intended for THM modelling in rocks (ROCMAS, FRACON, THAMES and AQCLAY) regarding the THM formulation that is used in each of them. These programs were used for modelling the THM behaviour of Kamaishi Mine Heater Experiment. The main discrepancies among the programs are related to the treatment of the gas phase. In the case of CODE_BRIGHT [7,8], the program that is used in this paper, the formulation of balance equations was made based on the compositional approach and diffusion, dispersion and advection are explicitly considered in the gas phase. This means that vapour is transported by these various mechanisms of transport and all vapour fluxes imply energy transport.

In another contribution, Rutqvist et al. [9] and Rutqvist and Tsang [10] explore the possibilities of doing THM analyses by coupling TOUGH2 and FLAC3D in a sequential way. This approach is interesting because it exploits the capabilities of the TH approach and the M approach coming from two specialized programs. Couplings are introduced via external modules. One of the applications performed using THOUGH-FLAC is the problem of disposal of nuclear waste in an unsaturated fractured porous media. The stress field influences porosity, intrinsic permeability and capillary pressure. Anisotropy is considered because the intrinsic permeability variations depend on axis direction according to changes in the stress tensor. It is concluded that the sequential approach is sufficiently appropriate because the hydro-mechanical changes are slow in the examples investigated. A result regarding the importance of the couplings is that the thermo-hydrological problem shows moderate influence from the mechanical part.

In another context, there are various applications of THM problems using CODE_BRIGHT that should be mentioned. The THM applications are related to unsaturated soils and with temperatures limited below 100 °C because bentonitic clays considered in radioactive waste schemes may undergo structure changes if temperatures become too high. For instance, Gens et al. [11] report THM analyses to investigate the behaviour of an engineered clay barrier for radioactive waste disposal in granitic rock. In addition, Olivella and Gens [12] have investigated the vapour migration in low permeability clays. In this work, it was found that gas permeability plays an important role in the mobility of vapour in the gas phase. Also in this paper, a discussion on the effects of capillary pressure on phase change is performed. It is recognized that there are two approaches reported in the literature depending on the porous medium retention properties. In the geothermal reservoir (GR) approach, the small capillary effects are neglected and this implies the absence of a retention curve and, therefore, degree of saturation is obtained from enthalpy balance. In contrast, the non-isothermal unsaturated soil (NUS) approach is based on the assumption that degree of saturation is given by the retention curve and it is a function of capillary pressure. In this paper, the NUS approach is used. It is interesting to note, however, that the fractured tuff in which the DST test was performed contains fractures that desaturate at very low capillary pressures (few kPa) while the matrix has smaller pores and requires higher capillary pressures to desaturate (hundreds of kPa).

This paper presents coupled THM analyses based on the DST in situ test configuration. The coupled THM analyses have been performed in two dimensions using CODE_BRIGHT and a double structure is considered by means of superposition of meshes. Comparison with measurements of temperatures and gas permeabilities is performed. Former, analyses of the DST test with CODE_BRIGHT using single structure have been described elsewhere [13,14] and were considered as a first step towards this modelling work. For space reasons, the single structure calculations are not included here. Results from this single structure modelling are also used for comparison purposes by Rutqvist et al. [15].

2. THM formulation and code description

The governing equations for the THM problem are balance equations and constitutive equations. Mass conservation equations apply to water and air. When the porous medium is deformable, the momentum balance equation (mechanical equilibrium) is also taken into account. In non-isothermal problems, the internal energy balance for the total porous medium must be considered. The basic equations solved by the finite element code CODE_BRIGHT are:

Mechanical equilibrium equations (1, 2 or 3 dimensions)

$$\nabla \cdot \boldsymbol{\sigma} + \mathbf{b} = 0, \tag{1}$$

where $\boldsymbol{\sigma}$ is the stress tensor and $\mathbf{b}$ is the body forces vector. This equation should be combined with a mechanical constitutive model (stress–strain equation) and the strain–displacement equations.

Conservation of component i is expressed in the following way:

$$\frac{\partial}{\partial t}(\omega_{\mathrm{l}}^{i}\rho_{\mathrm{l}}S_{\mathrm{l}}\phi+\omega_{\mathrm{g}}^{i}\rho_{\mathrm{g}}S_{\mathrm{g}}\phi)+\nabla\cdot(\mathbf{j}_{\mathrm{l}}^{i}+\mathbf{j}_{\mathrm{g}}^{i})=f^{i},\quad i=w,a, \tag{2}$$

where ω is the mass fraction, ρ is the density, ϕ is the porosity, S is the degree of saturation, $\mathbf{j}$ are the total fluxes and f^{i} is a source–sink term. Subscripts l or g correspond to liquid or gas phase, respectively. Superscript $i=w$ or a leads to water or air balance, respectively. The mass balance equations should be combined with constitutive equations and equilibrium restrictions. Darcy's law and Fick's law are used for the calculation of the fluxes, respectively, for the phases and for the components.

Internal energy balance is written as

$$\frac{\partial}{\partial t}(E_{\mathrm{s}}\rho_{\mathrm{s}}(1-\phi)+E_{\mathrm{l}}\rho_{\mathrm{l}}S_{\mathrm{l}}\phi+E_{\mathrm{g}}\rho_{\mathrm{g}}S_{\mathrm{g}}\phi)+\nabla\cdot(\mathbf{i}_{c}+\mathbf{j}_{E\mathrm{s}}+\mathbf{j}_{E\mathrm{l}}+\mathbf{j}_{E\mathrm{g}})=f^{Q}, \tag{3}$$

where E is the internal energy, $\mathbf{j}_{E}$ are fluxes of internal energy and f^{Q} is a source/sink term of heat. More details of the formulation and numerical method can be found elsewhere [7,8].

3. Double structure approach

The specific nature of the host rock (fractured tuff) makes it necessary to recognize that double porosity and, hence, double permeability play a role in the hydrological problem. Hydraulic properties that correspond to the tuff are summarized in Table 1, mechanical and thermal properties are summarized in Table 2. Three units are distinguished in the rock and are referred to in this paper as: Lower, Intermediate (where the drift was excavated) and Upper. These correspond, respectively, to the units tptpll, tptpmn and tptpul referred in other works.

The intrinsic permeabilities together with relative permeability (calculated using the van Genuchten [16] parameters for retention curve) permit to obtain a function of permeability versus capillary pressure that is represented in Figs. 1 and 2, respectively, for the liquid and for the gas. The curve is obtained by adding the contribution of the matrix and the fracture. This plot of

Table 1
Tuff hydraulic properties for the lower, intermediate and upper rock units considered

Property	Lower		Intermediate		Upper	
	Matrix	Fractures	Matrix	Fractures	Matrix	Fractures
Porosity (dimensionless)	0.13	0.00329	0.11	0.00260	0.154	0.00171
Intrinsic permeability (m^2)	0.247×10^{-15}	0.187×10^{-11}	0.124×10^{-16}	0.100×10^{-12}	0.525×10^{-17}	0.635×10^{-12}
Capillary pressure parameter (P_{o}) in VGM for retention curve (MPa)	0.354	0.0602	0.444	0.01027	0.0943	0.006369
Shape parameter (m) in VGM for retention curve	0.207	0.492	0.247	0.492	0.243	0.492
Residual saturation in VGM for retention curve	0.08	0.0	0.18	0.0	0.06	0.0
Shape parameter (m) in VGM for liquid relative permeability (k_{rl})	0.207	0.492	0.247	0.492	0.243	0.492
Gas relative permeability (k_{rg})	$1-k_{\mathrm{rl}}$	S_{g}^{3}	$1-k_{\mathrm{rl}}$	S_{g}^{3}	$1-k_{\mathrm{rl}}$	S_{g}^{3}

VGM, Van Genuchten model.

Table 2
Tuff thermal and mechanical properties for the lower, intermediate and upper rock units considered

Property	Lower	Intermediate	Upper
Porosity (dimensionless)	0.13	0.11	0.154
Dry thermal conductivity (W/mK)	1.59	1.67	1.15
Saturated thermal conductivity (W/mK)	2.29	2.10	1.70
Solid phase specific heat (J/kg K)	865	865	865
Elastic modulus (MPa)	36,800	36,800	36,800
Poisson modulus (dimensionless)	0.2	0.2	0.2
Thermal expansion coefficient (K^{-1})	0.2×10^{-4}	0.2×10^{-4}	0.2×10^{-4}

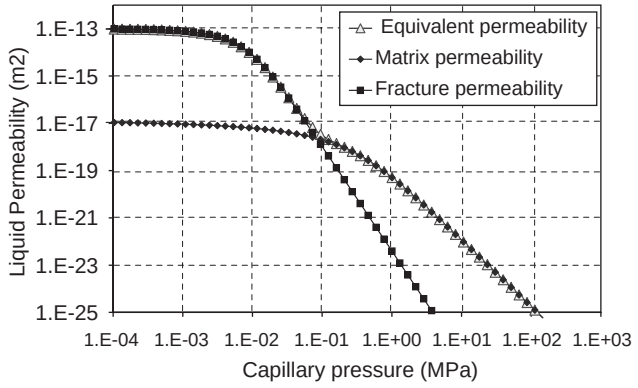

Fig. 1. Liquid permeability as a function of capillary pressure (intermediate rock unit).

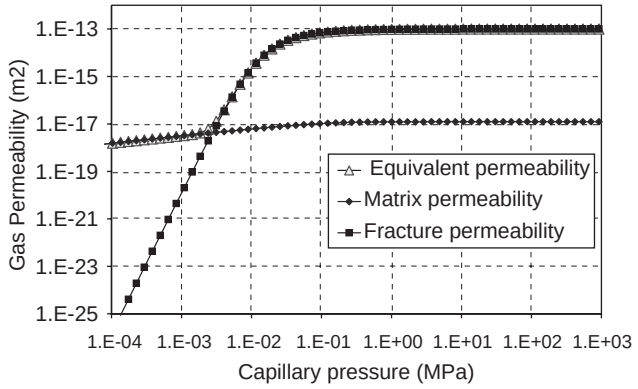

Fig. 2. Gas permeability as a function of capillary pressure (intermediate rock unit).

equivalent permeability was very useful for approximating an equivalent permeability function for single structure analyses [14]. Here, it is not necessary to perform any simplification because matrix and fractures are considered separately.

Figs. 1 and 2 show that the rock matrix, although it is less permeable, may be dominant depending on the capillary pressure. This happens for both, the liquid and the gas phases. The field test undergoes large variations of capillary pressure in space and time. For instance, high capillary pressures develop near the drift due to strong drying induced by heating.

Diffusion of vapour is calculated in the following way:

$$\mathbf{i} = -\tau\varpi(\phi S_g)\rho_g D(T, P_g)\mathbf{I}\nabla\omega_g^w, \tag{4}$$

where $\tau = 1$ is a tortuosity coefficient, $\varpi = S_g^{-n}$ is an enhancement factor, (ϕS_g) is an estimation of the available area for diffusion, ρ_g is the gas density, $D(T, P_g)$ is the molecular diffusion coefficient for vapour which depends on temperature and gas pressure, $\mathbf{I}$ is the identity matrix, and ω_g^w is the mass fraction of vapour in the gas phase. Vapour diffusion takes place through the rock matrix due to the higher porosity of the matrix. The enhancement factor for vapour diffusion is justified by several factors, i.e.: meniscus are short-cuts for vapour migration [17], the temperature gradients are locally higher than the average value in the porous medium [17] and, finally, the gas permeability is high so the dry-air is stationary (in a closed system, dry-air/vapour binary diffusion induces an advective gas flow that maintains the dry-air stationary) [12,18]. The enhancement factor is calculated as a function of gas degree of saturation. The value of the power n has been set to 1 which means that vapour diffusion is highly efficient even at high water contents.

The heat power introduced in the calculations in two dimensions corresponds to both the heaters in the drift and the wing heaters in the sidewall boreholes. Since the model is 2D (per metre in the axial direction), the following values have been considered:

Heat power in canister-heaters

$$\begin{aligned} Q(\mathrm{W/m}) &= Q_{\mathrm{total}}/(n \times s) \\ &= 36,400\,\mathrm{W}/(9\ \mathrm{canister} \times 4.7\,\mathrm{m}) \\ &= 860\,\mathrm{W/m}. \end{aligned}$$

Heat power in inner wing-heaters

$$\begin{aligned} Q(\mathrm{W/m}) &= Q_{\mathrm{total}}/(n \times s) \\ &= 37,520\,\mathrm{W}/(50\ \mathrm{wings} \times 1.87\,\mathrm{m}) \\ &= 401\,\mathrm{W/m}. \end{aligned}$$

Heat power in outer wing-heaters

$$\begin{aligned} Q(\mathrm{W/m}) &= Q_{\mathrm{total}}/(n \times s) \\ &= 55,300\,\mathrm{W}/(50\ \mathrm{wings} \times 1.87\,\mathrm{m}) \\ &= 591\,\mathrm{W/m}. \end{aligned}$$

The total power (Q_{total}) is divided by the number of heaters (n) and the associated length (s). The total power corresponds to 70% of the nominal power. This reduction is based on a 3D–2D comparison for the linear heat flow problem. An average reduction coefficient of the power is applied according to an exponential decay law ($Q = Q_o \exp(-\alpha t)$). The exponential coefficient has been set to $\alpha = 0.07884\,\mathrm{yr}^{-1}$ on the basis of the actual decay of supplied power. The power is distributed among the nodes in the corresponding length; however, 1D elements with high thermal conductivity and without hydraulic properties connect the nodes in the drift wall and connect the nodes inside the inner heater wing and also inside the outer heater wing. The inner and the outer heater wings are not connected with such 1D elements.

Fig. 3 shows the geometry and the conceptual double structure approach. Fig. 4 shows the finite element mesh which is duplicated to consider the matrix and the fractures. It can be observed that the concrete invert has also been considered in the simulation. Since a 2D

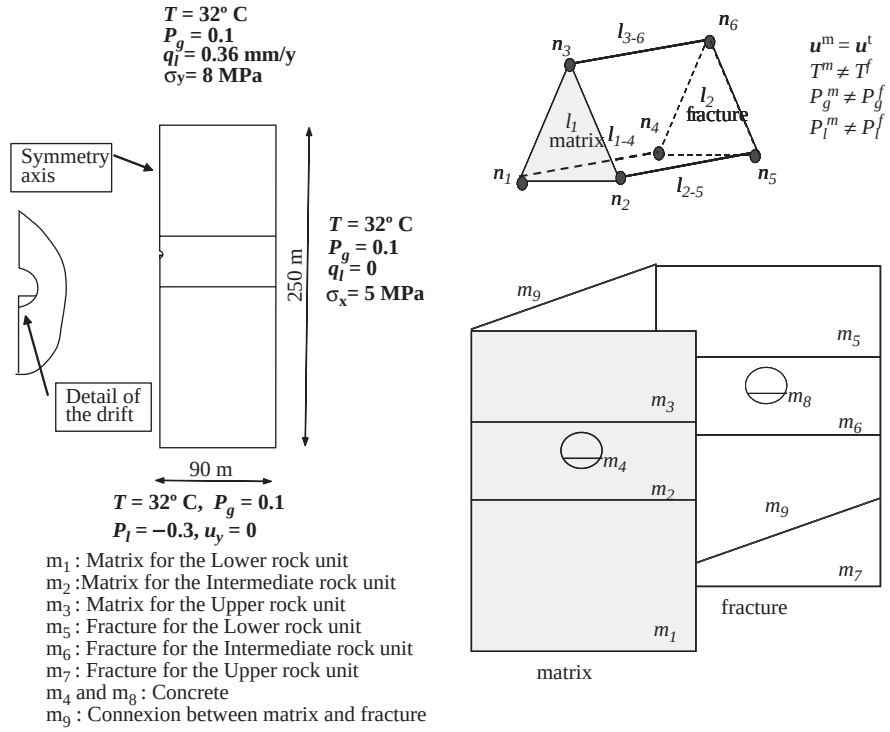

Fig. 3. Geometry and boundary conditions for THM calculations and detail of the approach for the treatment of the double structure using two superimposed domains.

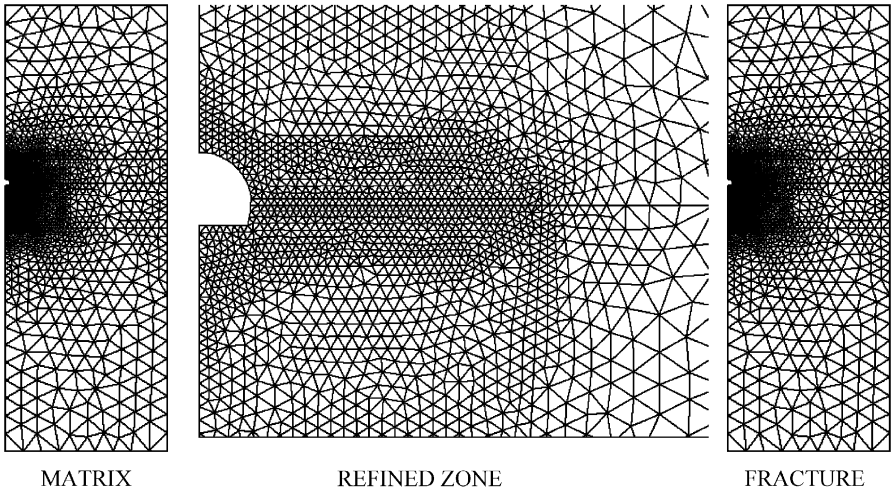

Fig. 4. Finite element mesh composed by 6508 nodes. Half of the nodes belong to the matrix and half belong to the fracture. In addition to the 2D triangle elements, each pair of nodes is connected by a 1D element.

analysis usually corresponds to 1 m in the out of plane direction, the model here uses 0.5 m for the thickness of each mesh.

1D elements connect the matrix and the fracture. Each 1D element connects two nodes, one node in the matrix and another in the fracture. The transport properties of the connection elements (i.e., hydraulic conductivity, thermal conductivity and vapour diffusion) are equal to the properties of the matrix and the travel distance between the matrix and the fracture (length of the 1D elements) is set to 0.01 m. These connection elements do not have volume, i.e., do not store mass or energy. However, for each node, the cross-sectional area of the corresponding 1D element is set as the area of the 2D cell associated to the node. The area of the 2D cell associated to each node is obtained by

means of the integral of the differential area times the finite element 2D shape function associated to the node. In this way, the connection is independent of the refinement of the mesh because, although there are more connections in the zone of refined elements, the associated areas are smaller in these refined zones.

Due to the short length of the 1D elements, there is practically equilibrium between the matrix and the fracture (same pressure and temperature). However, due to the different retention curves considered for the matrix and the fracture, the initial degree of saturation is ~92% (matrix) and ~5% (fracture) at the drift horizon. Longer lengths of the connection elements could be used to represent larger spacing between fractures and, in such case, pressures and temperatures would tend to be different in the two media.

A key point in the model presented in this paper is the mechanical coupling. Generally speaking, the coupling between the mechanical and the hydraulic problem can take place in different ways. One of the couplings that may be relevant for the DST test is the variation of intrinsic permeability induced by porosity changes.

Porosity changes induced by volumetric strains are distributed equally between the matrix and the fracture in this work. This can be written in the following way:

$$\begin{aligned}
&\Delta\phi = \Delta\phi_{\text{matrix}} + \Delta\phi_{\text{fracture}} = (1 - \phi_{\text{matrix}} - \phi_{\text{fracture}})\Delta\varepsilon_v,\\
&\Delta\phi_{\text{matrix}} \approx \left(\frac{1}{2} - \phi_{\text{matrix}}\right)\Delta\varepsilon_v = (1 - 2\phi_{\text{matrix}})\Delta\varepsilon_v/2,\\
&\Delta\phi_{\text{fracture}} \approx \left(\frac{1}{2} - \phi_{\text{fracture}}\right)\Delta\varepsilon_v = (1 - 2\phi_{\text{fracture}})\Delta\varepsilon_v/2,
\end{aligned} \tag{5}$$

where it can be seen that the sum of the two variations of porosity, respectively, for the matrix and for the fracture equals the total variation of porosity. This latter is proportional to the total volumetric strain variation. Compression or dilation can be considered for volumetric strain and this will lead to reduction or increase of porosity, respectively. Obviously, assuming an equal distribution of deformations between fracture and matrix is a simplifying approximation. Different distributions could be considered but this depends also on the mechanical constitutive model used. Here, the thermo-elastic approach is considered, which can be written as

$$\begin{aligned}
&\Delta\varepsilon_v = \frac{\Delta p}{K} + 3\alpha\Delta T, \quad K = \frac{E}{3(1-2v)},\\
&\Delta\varepsilon_s = \frac{\Delta q}{3G}, \quad G = \frac{E}{2(1+v)},
\end{aligned} \tag{6}$$

where E, v, K, G are elastic parameters, α is the thermal expansion coefficient, T is the temperature, and p and q are stress invariants (respectively, mean stress and deviatoric stress).

Fracture aperture may be related with porosity associated to the fractures, i.e., $\phi_{\text{fracture}} = b/s$, where b is the aperture and s the spacing between fractures if a family of parallel fractures is considered. The fact that porosity and aperture are proportional permits to conclude that the cubic law ($k = b^3/(12s)$) of intrinsic permeability [19] and Kozeny's law are equivalent if written in the following way:

$$\mathbf{k}_{\text{f}} = \mathbf{k}_{\text{of}} \frac{\phi_{\text{f}}^3}{(1-\phi_{\text{f}})^2} \frac{(1-\phi_{\text{of}})^2}{\phi_{\text{of}}^3} \approx \mathbf{k}_{\text{of}} \frac{\phi_{\text{f}}^3}{\phi_{\text{of}}^3} = \mathbf{k}_{\text{of}} \frac{b_{\text{f}}^3}{b_{\text{of}}^3}, \tag{7}$$

where ϕ_{f} is the fracture porosity (ϕ_{of} is a reference value for ϕ_{f}), b_{f} is the fracture aperture (b_{of} is a reference value for b_{f}) and $\mathbf{k}_{\text{f}}$ is the intrinsic permeability due the presence of fractures ($\mathbf{k}_{\text{of}}$ is a reference value for $\mathbf{k}_{\text{f}}$). The first part of Eq. (7) (Kozeny's law) is applied either to the matrix or to the fracture. However, volumetric deformation has different effect on permeability depending on the porosity ranges. In this problem, volumetric strains are relatively small and are caused by the combined thermo-mechanical effect. For low porosities (as happens in the fracture where porosity is less than 0.004) the changes of permeability are significant while for high porosities (as happens in the matrix where porosity is higher than 0.10) the changes of permeability are negligible. The approach followed in this paper implies heterogeneous and isotropic permeability distribution as deformation progresses. Finally, capillary pressure is not modified by changes in porosity or aperture as proposed by Rutqvist and Tsang (2003) [3]. This could be included and would imply a moderate decrease of retention properties in the fracture. A factor for capillary pressure variation can be calculated from permeability changes as cubic law, $k = b^3/(12s)$, and Laplace's law, $p_{\text{g}} - p_{\text{l}} = 2\sigma/b$, are combined. The variation of intrinsic permeability expected in this problem is less than one order of magnitude and this implies a variation of the capillary pressure by a factor less than 2.

4. Analyses performed

In this section, the results obtained in a set of three cases are presented and compared with temperature and gas permeability measurements. The main objective of the paper was to investigate the effects of mechanical coupling on the thermo-hydrological calculations. In order to show the effect of such coupling, three cases are described. The first one corresponds to minimum coupling because intrinsic permeability is considered constant, i.e., does not change with deformations. The mechanical problem is solved using the linear standard thermo-elastic model described above (Eq. (6)), however, leading to small porosity variations. The second

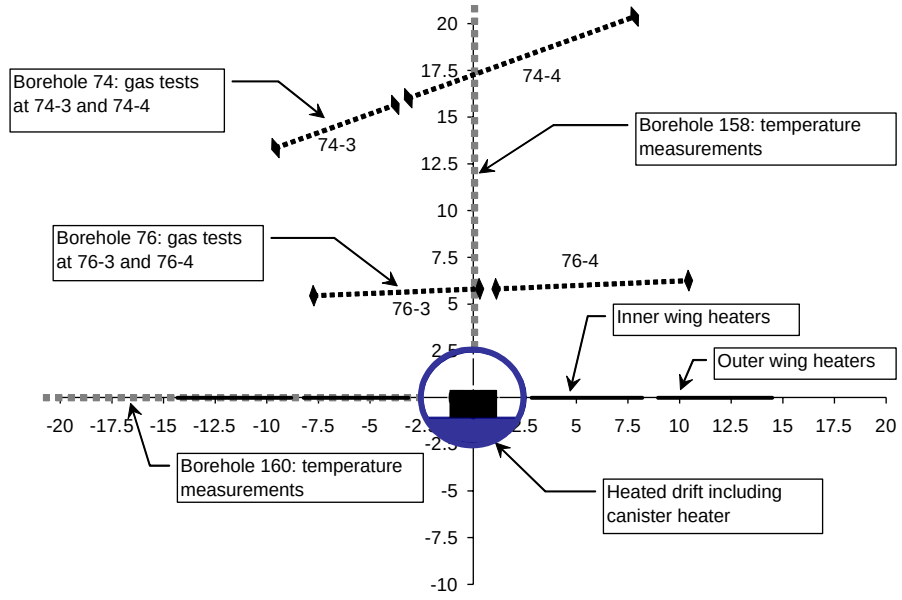

Fig. 5. Location of instrumentation for temperature (Boreholes 158 and 160) and gas permeability measurement (Boreholes 74 and 76).

case includes intrinsic permeability variations via the cubic law (Eq. (7)), and deformations are calculated in the same way (Eq. (7)). Finally, the third case presented in this section, includes intrinsic permeability variations via cubic law too, but deformations are calculated with a thermo-elastic model modified with a dilatancy term.

Fig. 5 shows a schematic representation of the section of the test with the location of measurements considered. Boreholes 158 and 160 contain temperature sensors installed every 30 cm. This means that, e.g., 158–55 and 160–55 are situated at 16.5 m ($55 \times 0.30\,m^2$) away from the drift wall.

Fig. 5 shows also the position for gas permeability tests at Boreholes 74 and 76, each one displaying two intervals for gas permeability measurements. Boreholes 57 and 59 are situated in a similar position as 74 and 76 but in a different vertical section. In this way, if the host rock was homogeneous, 57–3 and 57–4 would show similar behaviour as 74–3 and 74–4, respectively, and 59–3 and 59–4 would show similar behaviour as 76–3 and 76–4, respectively.

4.1. Constant intrinsic permeability (BASE CASE)

This section shows the results of a THM simulation with moderate coupling between the thermo-hydraulic (TH) and the mechanical problem (M). Although the mechanical part is included (thermo-elastic behaviour), the intrinsic permeability is considered constant, i.e., independent on the changes of deformations in each medium.

The calculated temperature for the 4 years modelling can be compared with measurements available. Fig. 6 shows the computed temperature evolution up to 4 years of heating compared with measurements for the Boreholes 158 (vertical from drift roof) and 160 (horizontal from drift wall). The

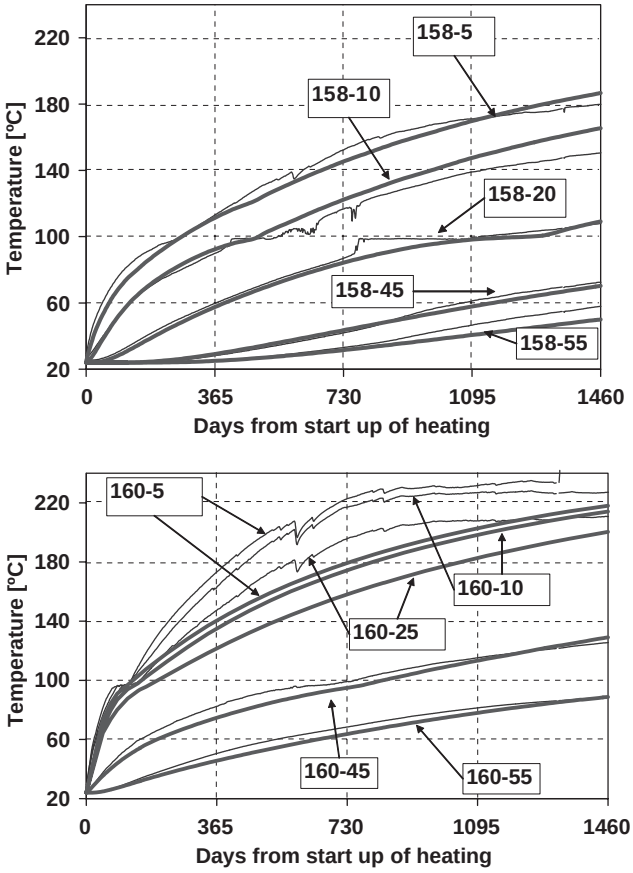

Fig. 6. Calculated (thick lines) and measured (thin lines) temperatures for selected points in Boreholes 158 and 160. BASE CASE.

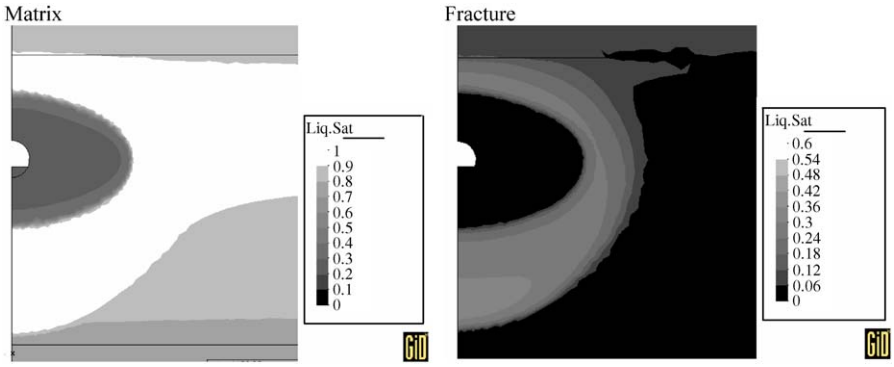

Fig. 7. Calculated saturation at 4 years. Matrix saturation using 0–1.0 range. Fracture saturation using 0–0.6 range. BASE CASE.

calculated and measured temperatures agree well for Borehole 158. For 158–10 and for 158–20, temperature remains constant for some days at 100 °C in both measurements and calculations. This is an evidence of the water phase change which is associated with the consumption and transport of the latent heat by the water. Phase change is also evident in Borehole 160. All the points, except the one located farther away (168–55) undergo some temperature stabilization at 100 °C.

Temperatures show the largest discrepancies at points 160–5, 160–10 and 160–25. These sensors are located at 1.5, 3 and 7.5 m from the drift wall in the horizontal direction and, therefore, these sensors measure temperatures very close the wing heaters. The wing heaters are discrete sources separated 1.87 m from each other in the drift axis direction. This is not considered in the 2D vertical model and, consequently, the calculated temperatures are smoothed locally.

The distributions of degree of saturation at 4 years for the matrix and the fracture are shown in Fig. 7. Due to heating, a dried zone has developed that affects both matrix and fracture. As water evaporates, it migrates (diffusion plus gas phase advection) and condenses thus creating a zone of higher saturation which is affected by the gravity. A liquid water flux towards the drift appears because the high capillary pressures developed in the dried zone. Since liquid relative permeability is reduced this flow back is not able to equilibrate the vapour migration.

Finally, Fig. 8 shows the calculated and measured gas permeability variations. This is defined as the gas permeability ratio between the current value and the initial value before heating. In the analysis presented in this section, gas permeability variations are only caused by the relative permeability variations induced by changes in degree of saturation. It can be observed that for points near the drift (see Borehole 76 in Fig. 5) gas permeability decreases first and then increases again. This indicates that a higher saturation front advances. For points in a position far from the drift (see Borehole 74 in Fig. 5) gas permeability tends to decrease very moderately and this means that the saturation front has not reached these points.

4.2. Variable intrinsic permeability (CASE 1)

The analysis presented in this section uses variable intrinsic permeability and the mechanical problem is solved using conventional thermo-elasticity. Thermal expansion induces changes in the stresses and the variations of porosity depend not only on the elastic parameters (Young's modulus, Poisson's ration and thermal expansion coefficient) but also on the boundary conditions and the presence of the drift. In a porous rock free of stresses and without confinement, thermal expansion would not tend to change porosity, in principle. However, if the rock was fully confined, then the only available space for solid expansion would be the pores. These are two extreme cases; and the DST test corresponds to an intermediate situation. If, e.g., displacements are not permitted along the external boundaries, porosity reduces more than in the case of constant stress on top and lateral boundaries. This latter case has been considered here as indicated before.

In summary, thermo-mechanical effects cause porosity variations and this induces intrinsic permeability variations. Kozeny's law is used for both the matrix and the fracture. Eqs. (5) are used to calculate porosity variations and Eq. (7) is used for intrinsic permeability. Intrinsic permeability shows significant variations in the fracture and negligible variations in the matrix because the fracture has much lower porosity (given by the fracture aperture).

Figs. 9–11 show temperatures, degree of saturation and gas permeability. It can be seen that temperatures are somewhat higher than in the BASE CASE and this is caused by the reduction in the overall water movement induced by intrinsic permeability reduction. If water and gas flow are reduced, heat advection is also reduced and this implies higher temperatures. In principle, tempera-

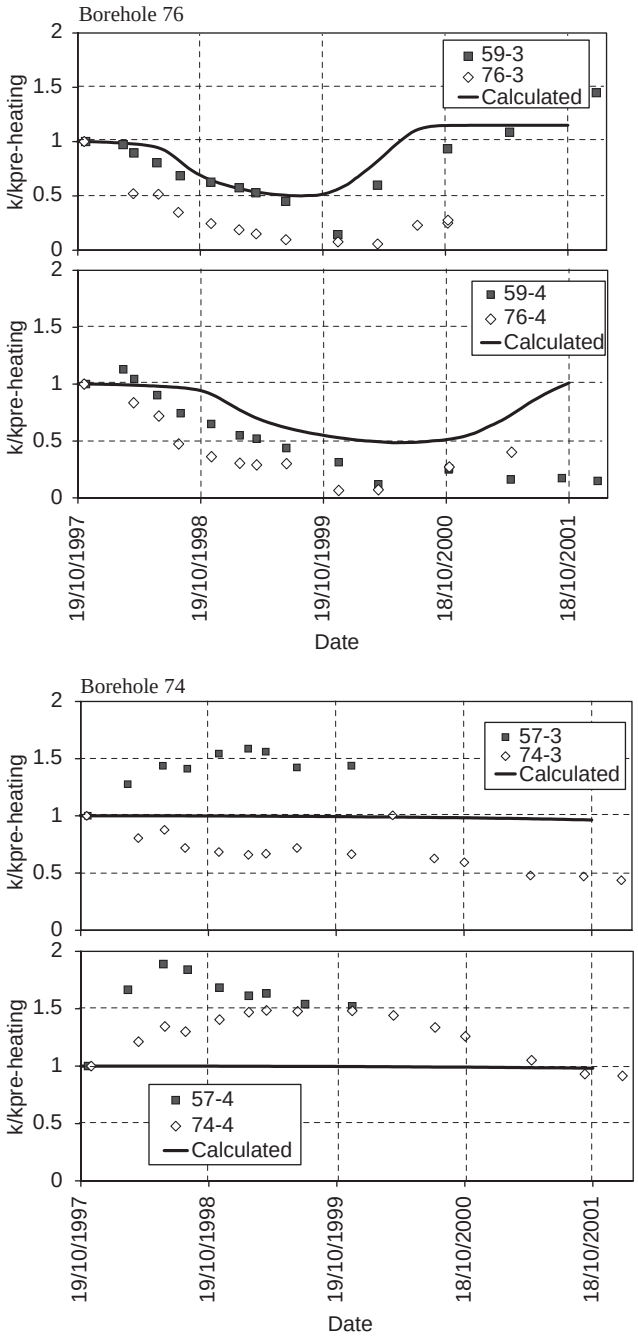

Fig. 8. Measured and calculated gas permeability variations. BASE CASE.

ture could also show the influence of thermal conductivity variations but the degree of saturation in the matrix is quite similar in both cases and therefore the temperature differences are attributed to differences in energy advection. Degree of saturation in the fracture shows higher values than in the previous case and this implies an increase of liquid relative permeability and a further decrease of gas permeability. However, degree of saturation in the fracture does not affect thermal conductivity in the rock due to its low porosity.

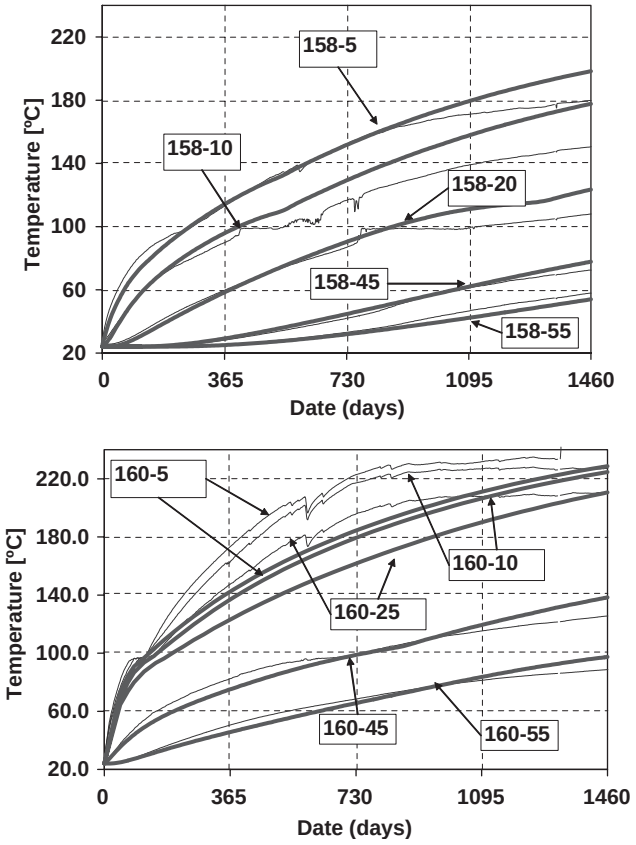

Fig. 9. Calculated (thick lines) and measured (thin lines) temperatures for selected points in Boreholes 158 and 160. CASE 1.

Gas permeability shows now the combined hydraulic and mechanical effects. The saturation front is still observed in Borehole 76, but permeability reduces more than in the BASE CASE due to intrinsic permeability reductions induced by mechanical effects. This is more evident in Borehole 74 for which hydraulic effect was very moderate while now porosity reduction induces significant changes in permeability. Gas relative permeability is generally lower in this case because of the higher water content in the fracture.

4.3. Variable intrinsic permeability (CASE 2)

The analysis presented in this section uses again variable intrinsic permeability in the same way as before but now the mechanical problem is solved in thermo-elasticity including dilatancy. This is a simplification because plasticity would be required if dilatancy had to be included, generally. However, as a first approximation, dilatancy in considered a function of the elastic deviatoric strains.

A simplified model has been used. The basic assumption is that shearing induces dilatancy. Elastic volumetric strain is then calculated in terms of the stress

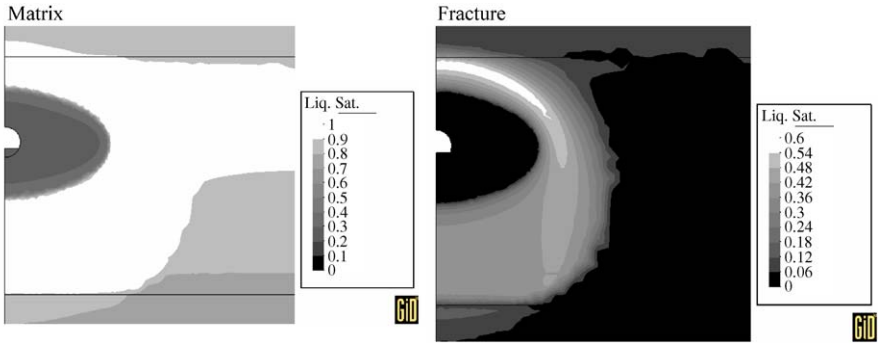

Fig. 10. Calculated saturation. Matrix saturation using 0–1 range. Fracture saturation using 0–0.6 range. CASE 1.

invariants p and q in the following way:

$$\Delta\varepsilon_v = \frac{\Delta p}{K} + \frac{(\tan\psi)\Delta q}{3G} + 3\alpha\Delta T, \tag{8}$$

where ψ is a dilatancy angle. A value of 24° for the dilatancy angle has been considered in the calculations. Using this model, permeability will increase or decrease depending on the shearing occurring in the different zones. Compression by mean stress increase still induces porosity reduction but the combined effect of compression and dilatancy may lead to zones where permeability decreases and zones where it increases. Furthermore, strains change with time because temperature increases with time. The type of model described in Eq. (8) was proposed in [20] for anisotropic elastic soils.

Temperatures, degree of saturation and gas permeability are plotted in Figs. 12–14. This case shows temperatures in between the two previous cases (BASE CASE and CASE 1). This means that, globally, heat flow due to water flow is higher than in CASE 1 but somewhat lower than in the BASE CASE. The degree of saturation distribution, both for the matrix and the fracture, is rather close to the BASE CASE.

Gas permeability results show a significant improvement (Fig. 14). A comparison of CASE 2 with the BASE CASE and with CASE 1, evidences that CASE 2 contains mechanical effects in a more appropriate way. For Borehole 76, the calculated evolution of gas permeability corresponds well with measurements except for the permeability increase measured at 59–3 which seems to indicate a local heterogeneity. For Borehole 74 dilatancy plays a significant role because this is the only calculation that permits the reproduction of the gas permeability increase shown by the measurements during the 1st and 2nd year. According to the model, permeability increases first due to shearing and afterwards it decreases due to compression induced by heating.

5. Conclusions

A double structure calculation has been considered in order to investigate the THM behaviour of the DST test at Yucca Mountain. The model is mainly based on previous TH calculations published in the literature [3] and on single structure THM calculations performed by the authors [14]. Comparison with temperatures and gas permeabilities has been possible because the authors participated in an international benchmarking exercise in the context of DECOVALEX-III project. The main phenomenon that has been considered in this work is the influence of mechanical effects on the thermal–hydrological problem.

The double structure approach is more appropriate to model the DST test than the single structure for several reasons: (a) hydrological calculations are more realistic because the advective fluxes are more consistent due to independent permeability functions considered for the matrix and the fracture which are related to different retention curves, (b) the characteristic temperature signature due to water phase change is captured better than in single structure calculations, (c) intrinsic permeability variations with deformation can be introduced in a more consistent way, specially because they should be attributed to the fractures rather than to the matrix.

In order to have a reference analysis, a BASE CASE calculation was performed by assuming that intrinsic permeability was not dependent on the mechanical part. As permeability variations were incorporated (CASE 1), it has been shown that using standard thermo-elastic behaviour, the reduction of permeability due to compression was sufficient to modify the moisture distribution, especially in the fracture. The flux of water was reduced because of the intrinsic permeability reduction but at the same time relative permeability was higher due to higher water saturation in the fracture. However, the temperature field indicates that globally there was less energy transported by advection. In CASE 1, both liquid and gas permeability were smaller. Intrinsic permeability reduction implies also less evidence of the water phase change and the periods of temperature stabilization were reduced.

When comparing temperatures and gas permeabilities with measurements in CASE 1, there are two aspects that

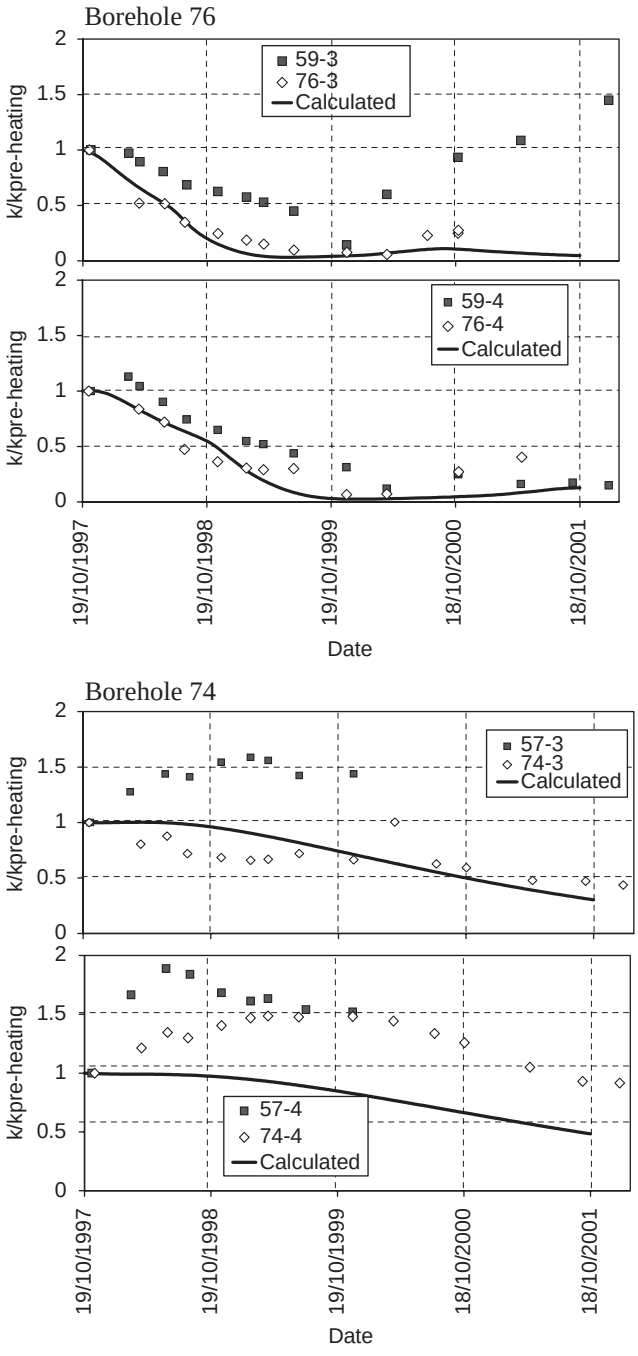

Fig. 11. Measured and calculated gas permeability variations. CASE 1.

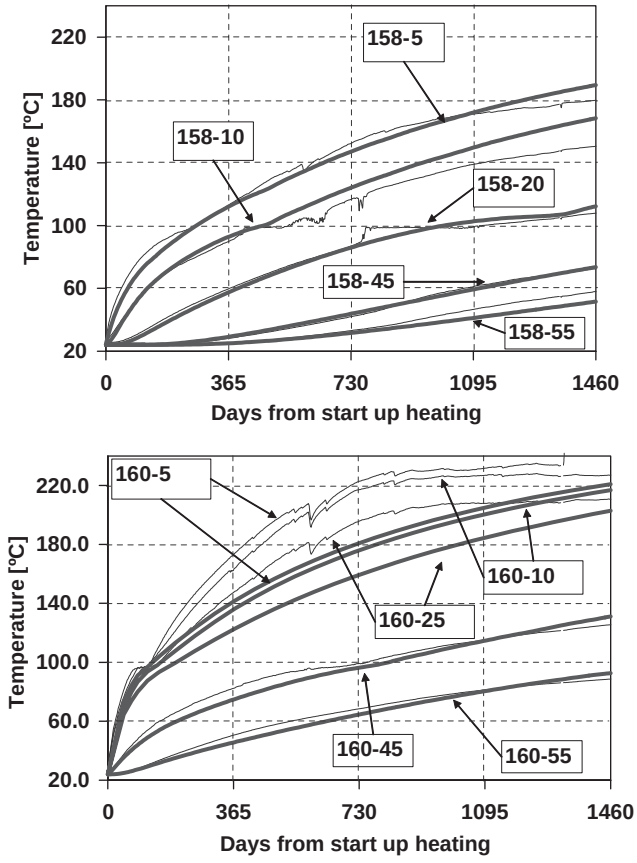

Fig. 12. Calculated (thick lines) and measured (thin lines) temperatures for selected points in Boreholes 158 and 160. CASE 2.

seem to indicate that intrinsic permeability reduction was not fully realistic. Firstly, the temperature stabilization periods at 100 °C were shorter, and secondly, calculated gas permeability reduced more than in the measurements. Both aspects led to conclude that reduction of intrinsic permeability was overestimated.

The third analysis presented in the paper incorporates a modified version of elasticity which includes dilatancy (CASE 2). This analysis leads to a quite different distribution of intrinsic permeability variations, with zones in which intrinsic permeability reduces because compression dominates and zones where intrinsic permeability increases because dilatancy dominates. The overall behaviour obtained is improved and the gas permeability model predictions show encouraging agreement with measurements, even for the zones were hydrological effects are small.

Finally, it can be concluded that in the case of DST test at Yucca Mountain, several types of THM couplings take place. The mechanical problem has been solved considering a simplified model and the intrinsic permeability variations induced by deformations have been introduced. This permits a coupling from mechanical to hydraulic and in turn to thermal. The cases analysed show that both temperatures and gas permeabilities are influenced by deformations. The model is able to reproduce the measured gas permeability variations when dilatancy induced by shearing is included. Temperature predictions indicate that there could be a mechanical process (dilatancy) that tends to increase intrinsic permeability at least to compensate the compression induced by volumetric thermal expansion of the rock.

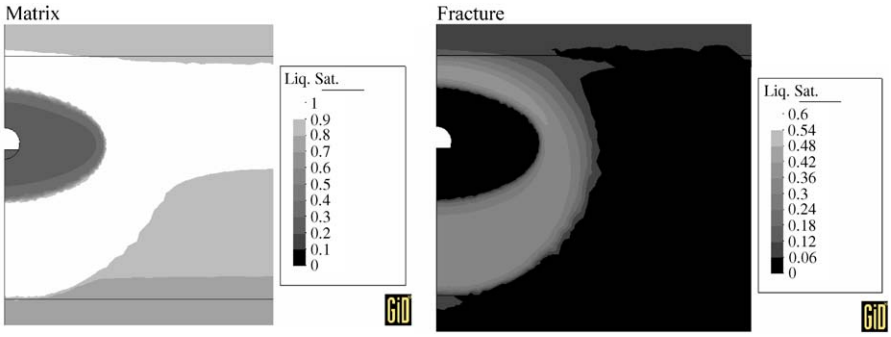

Fig. 13. Calculated saturation. Matrix saturation using 0–1.0 range. Fracture saturation using 0–0.6 range. CASE 2.

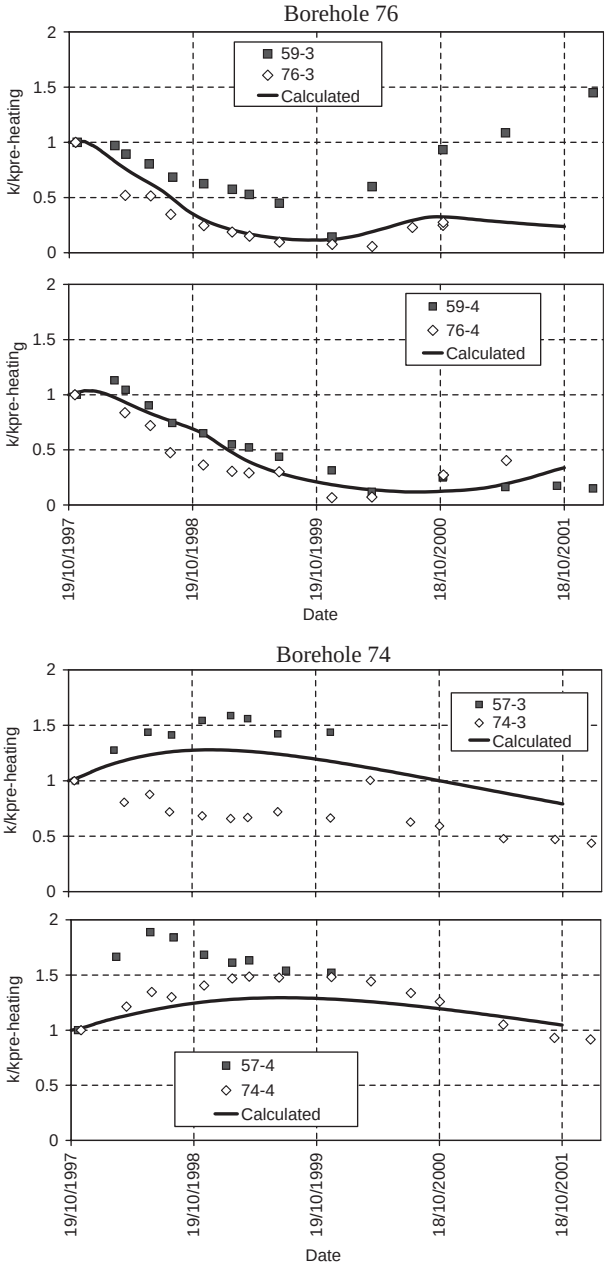

Fig. 14. Measured and calculated gas permeability variations. CASE 2.

Acknowledgements

The authors would like to acknowledge ENRESA (Empresa Nacional de Residuos, S.A., Spain) for funding the participation in the international project DECOVALEX III.

References

[1] Civilian Radioactive Waste Management System. Ambient characterization of the Drift Scale Test Block. Las Vegas, NV: TRW Environmental Safety Systems Inc.; 1977.
[2] Civilian Radioactive Waste Management System. Drift Scale Test design and forecast results. Las Vegas, NV: TRW Environmental Safety Systems Inc.; 1977.
[3] Birkholzer JT, Tsang YW. Modelling the thermal–hydrologic processes in a large-scale underground heater test in partially saturated fractured tuff. Water Resour Res 2000;36:1431–47.
[4] Pruess K. TOUGH user's guide, Rep. LBL-20700. Berkeley, CA: Lawrence Berkeley National Laboratory; 1987.
[5] Pruess K. TOUGH2. A general purpose numerical simulator for multiphase fluid and heat flow, Rep. LBL-29400, UC-251. Berkeley, CA: Lawrence Berkeley National Laboratory; 1991.
[6] Rutqvist J, Borgesson L, Chijimatsu M, Kobayashi A, Jing L, Nguyen TS, Noorishad J, Tsang CF. Thermohydromechanics of partially saturated geological media: governing equations and formulation of four finite element models. Int J Rock Mech Min Sci 2001;28:105–27.
[7] Olivella S, Carrera J, Gens A, Alonso EE. Non-isothermal multiphase flow of brine and gas through saline media. Transp Porous Media 1994;15:271–93.
[8] Olivella S, Gens A, Carrera J, Alonso EE. Numerical formulation for a simulator (CODE_BRIGHT) for the coupled analysis of saline media. Eng Computations 1996;13:87–112.
[9] Rutqvist J, Wu YS, Tsang CF, Bodvarsson G. A modeling approach for analysis of coupled multiphase fluid flow, heat transfer, and deformation in fractured porous rock. Int J Rock Mech Min Sci 2002;39(4):429–42.
[10] Rutqvist J, Tsang CF. Analysis of thermal–hydrologic–mechanical behaviour near an emplacement drift at Yucca Mountain. J Contam Hydrol 2003;62–63:637–52.
[11] Gens A, Garcia-Molina A, Olivella S, Alonso EE, Huertas F. Analysis of a full scale in situ test simulating repository conditions. Int J Numer Anal Meth Geomech 1998;22(7):515–48.
[12] Olivella S, Gens A. Vapour transport in low permeability unsaturated soils with capillary effects. Transp Porous Media 2000;40:219–41.

[13] Datta RN. DECOVALEX III project report, Task 2A, final report. Thermal–hydrological modelling of the Yucca Mountain Project Drift Scale Test. Las Vegas, NV: Bechtel SAIC Company; 2003.

[14] Olivella S, Gens A, Gonzalez C. THM analysis of a heating test in a fractured tuff. In: Stephansson O, Hudson JA, Jing L, editors. Proceedings of the GEOPROC (Stockholm), coupled thermo-hydro-mechanical–chemical processes in geo-systems. Elsevier Geo-engineering Book Series; 2005. p. 181–6.

[15] Rutqvist J, Barr D, Datta R, Gens A, Millard A, Olivella S, Tsang C-F, Tsang Y. Coupled thermo-hydro-mechanical analysis of the Yucca Mountain Drift Scale Test—comparison of field results to predictions of four different models. Int J Rock Mech Min Sci 2005, this issue, doi:10.1016/j.ijrmms.2005.03.008.

[16] van Genuchten R. A closed-form equation for predicting the hydraulic conductivity of unsaturated soils. Soil Sci Soc Am J 1980:892–8.

[17] Philip JR, de Vries DA. Moisture movement in porous materials under temperature gradients. EOS Trans AGU 1957;38(2): 222–32.

[18] Bear J, Gilman A. Migration of salts in the unsaturated zone caused by heating. Transp Porous Media 1995;19: 139–56.

[19] Marsily de G. Quantitative hydrogeology: groundwater hydrogeology for engineers. San Diego and London: Academic Press; 1986.

[20] Graham J, Houlsby GT. Anisotropic elasticity of a natural clay. Geotechnique 1983;33(2):165–80.